

***I*-centered vs *F*-centered orthorhombic symmetry and negative thermal expansion of the charge density wave of EuAl₂Ga₂**

Harshit Agarwal^{1a}, Surya Rohith Kotla¹, Leila Noohinejad², Biplab Bag³, Claudio Eisele¹, Sitaram Ramakrishnan⁴, Martin Tolkieln², Carsten Paulmann², Arumugam Thamizhavel^{5b}, Srinivasan Ramakrishnan^{6c}, Sander van Smaalen^{1d}

¹*Laboratory of Crystallography, University of Bayreuth, Bayreuth, 95444, Germany*

²*P24, PETRA III, Deutsches Elektronen-Synchrotron DESY, Hamburg, 22607, Germany*

³*Department of Physics, Amity Institute of Applied Sciences, Amity University Jharkhand, Ranchi, 835303, India*

⁴*I-HUB Quantum Technology Foundation, Indian Institute of Science Education and Research, Pune 411008, India*

⁵*Department of Condensed Matter Physics and Materials Science, TIFR, Mumbai, 400005, India*

⁶*Department of Physics, Indian Institute of Science Education and Research, Pune 411008, India*

Abstract:

Together with EuGa₄ and EuAl₄, EuAl₂Ga₂ belongs to the BaAl₄ structure type with space group symmetry I4/mmm. EuAl₂Ga₂ develops an incommensurate charge density wave (CDW) at temperatures below T_{CDW} = 51 K. On the basis of temperature dependent single-crystal X-ray diffraction (SXRD) data, the incommensurately modulated CDW crystal structure of EuAl₂Ga₂ is determined to possess orthorhombic superspace symmetry *Immm(00γ)s00*. This symmetry is different from the orthorhombic *Fmmm* based symmetry of the CDW state of EuAl₄. Nevertheless, both symmetries *Immm(00γ)s00* and *Fmmm(00γ)s00* lead to the same conclusion, that the CDW is supported by the layers of Al1 type atoms, while the Eu and Al2 or Ga atoms are not directly involved in CDW formation. The different symmetries of the CDW states of EuAl₄ and EuAl₂Ga₂, as well as the observation of negative thermal expansion in the CDW state of EuAl₂Ga₂ might be explained by the effects of Ga substitution in the latter compound.

Keywords: Intermetallics, single crystal, charge density wave, phase transition

***Email:** ^aharshit.physics@gmail.com,

^bthamizh@tifr.res.in,

^cramky07@gmail.com,

^dsmash@uni-bayreuth.de

Introduction:

Quantum materials have played a significant role in condensed matter research for over a decade, delivering groundbreaking results [1]. Quantum materials refer to a class of materials that exhibit intriguing quantum mechanical properties at the nanoscale or atomic scale [2]. Due to the advent of coupled topological materials [3], our knowledge of emergent processes in quantum materials has improved significantly in recent years [4]. Intermetallic materials with a centrosymmetric square net structural motif having the BaAl_4 structure type [5] are ideal examples of quantum materials that exhibit superconductivity (SC), charge density wave (CDW) ordering, antiferromagnetism, and heavy fermionic behavior [6]. In Eu-based intermetallics, Eu has two types of valence states: Eu^{2+} (magnetic) and Eu^{3+} (nonmagnetic) due to an unstable $4f$ shell. Most Eu-based compounds exist in the divalent Eu^{2+} states and follow the RKKY interaction that causes the long-range magnetic ordering [7]. Similarly, Gd^{3+} ($4f^7$, $J=7/2$, $L=0$) based centrosymmetric intermetallic compounds follow RKKY interaction, giving rise to Fermi surface nesting [8].

A charge density wave (CDW) is a spatial modulation of electron charge density coupled to a modulation of the atomic positions (periodic lattice modulation, PLD) [9,10]. The origin of CDWs varies between materials but it can be classified according to the dimensionality of the band structure. In quasi-one-dimensional (1D) metals, the stabilization of CDW can be explained by the Peierls model, including Fermi surface nesting, metal-insulator transition, and periodic lattice distortion (PLD). In contrast, in 2D and 3D systems, CDWs occur due to q -dependent electron-phonon coupling, charge ordering, and PLD. However, the structural transition is common in all CDW materials [11]. The PLD leads to satellite reflections at distances $\pm q^{\text{CDW}}$ from the main Bragg reflections in single crystal X-ray diffraction studies (SXRD). The PLD introduces a new periodicity into the crystal and allows the analysis of CDW modulation [12]. In 3-D systems, first-order phase transition can be observed in physical properties, leading to incommensurate CDW. EuAl_4 [13], SrAl_4 [14], and $\text{R}_2\text{Ir}_3\text{Si}_5$ (where $\text{R} = \text{Ho}, \text{Er}$) [15,16] are examples of three-dimensional CDW compounds that show a thermal hysteresis in temperature-dependent electrical resistivity at the CDW transition temperature.

Compounds $\text{R}(\text{Al}_{1-x}\text{Ga}_x)_4$ ($\text{R} = \text{Sr}, \text{Eu}, \text{Ca}$) with the tetragonal BaAl_4 structure type with space group $I4/mmm$ have recently received interest, because of the discoveries of tetragonal to orthorhombic CDW transitions in EuAl_4 and SrAl_4 [14], of a square skyrmion lattice phase

in EuAl_4 [17–19], and of a tetragonal to monoclinic structural transition in CaAl_4 [20,21]. These materials show multiple antiferromagnetic transitions with topological hall effects. Eu-based compounds $\text{Eu}(\text{Al}_{1-x}\text{Ga}_x)_4$ reveal strong correlations between the structural, magnetic, and electronic properties [22,23]. These compounds contain three crystallographically independent atom sites where Ga preferably occupies one of the two independent Al sites **[Figure 1(a)]** [23]. EuAl_4 exhibits both the CDW at $T_{\text{CDW}} = 145$ K and orders antiferromagnetically below $T_{\text{N1}} = 15.4$ K with three successive antiferromagnetic transitions at $T_{\text{N2}} = 13.2$ K, $T_{\text{N3}} = 12.2$ K and $T_{\text{N4}} = 10.0$ K [24]. However, EuGa_4 orders antiferromagnetically below $T_{\text{N}} = 16.4$ K, but it develops a CDW only above a pressure of 2 GPa [24]. EuAl_4 contains skyrmions spin texture; it only requires the alternate stacking of the magnetic Eu layer and nonmagnetic Al layer [25]. Generally, skyrmions appear in non-centrosymmetric materials, but magnetic skyrmions lattice structures are studied in other centrosymmetric compounds like MnNiGa [26], Gd_2PdSi_3 [27], GdRu_2Si_2 [28], $\text{Gd}_3\text{Ru}_4\text{Al}_{12}$ [29] including EuAl_2Ga_2 [22]. Skyrmions can be stabilized in these centrosymmetric compounds without a geometrically frustrated lattice. BaNi_2As_2 hosts incommensurate and commensurate CDWs at 142 K and 137 K, respectively, and shows symmetry breaking from tetragonal to orthorhombic at 142 K and then a first-order triclinic structural transition at 137 K [30,31]. A phase diagram for $\text{BaNi}_2(\text{As}_{1-x}\text{P}_x)_2$ shows that electronic nematic fluctuations induce a tetragonal-to-orthorhombic phase transition with the incommensurate charge density wave in the material [32]. The coexistence of CDW and superconductivity is well established in Kagome-lattice compounds AV_3Sb_5 (A= K,Rb,Cs) [33], whereas the coexistence of CDW and magnetic order is well established in FeGe [34,35].

The temperature dependence of electrical resistivity shows an anomaly in EuAl_2Ga_2 , where the Al and Ga atoms split into two sublattices and create an ordered structure, that indicates a CDW state below 51 K [23]. The 3-dimensional CDW compound EuAl_2Ga_2 follows the RKKY interaction, having four antiferromagnetic transition temperatures: $T_{\text{N1}} \approx 19.5$ K, $T_{\text{N2}} \approx 15$ K, $T_{\text{N3}} \approx 11$ K, and $T_{\text{N4}} \approx 7$ K [22]. It also shows the persistence of the CDW in the magnetically ordered states [22]. The CDW modulation in EuAl_4 is orthorhombic with superspace group $Fmmm(00\gamma)s00$ [18]. However, the atomic positions and lattice parameters of the basic structure of the CDW phase obey the tetragonal symmetry [18]. Recent studies on the CDW structure of EuAl_4 propose the loss of local inversion symmetry by convergent beam electron diffraction [36]. Alternatively, centrosymmetric $Immm(00\gamma)s00$ superspace group

symmetry was proposed for the CDW state of EuAl_4 based on inelastic x-ray scattering experiments, but this model doesn't fit SXR data [37]. Resonant x-ray scattering (RXS) experiments on EuGa_2Al_2 have demonstrated the breaking of fourfold symmetry in CDW state that can be stabilized orthorhombic domains either $Immm(00\gamma)s00$ or $Fmmm(00\gamma)s00$ [38]. On the other hand, SrAl_4 shows an incommensurate CDW below $T_{\text{CDW}} = 243$ K, which has the non-centrosymmetric orthorhombic $F222(00\gamma)00s$ superspace group symmetry with modulation vector $q = (0, 0, 0.1116(2))$ at 200K [39].

A detailed structural description of CDW in EuAl_2Ga_2 has not yet been reported, and is presented here. We have found that CDW state of EuAl_2Ga_2 has an incommensurately modulated structure with orthorhombic superspace group $Immm(00\gamma)s00$, which differs from the symmetries of EuAl_4 and SrAl_4 . The presence of CDW modulation below the magnetic transition temperature of EuAl_2Ga_2 is also observed.

Experimental:

(A) Crystal Growth

Single crystals of EuAl_2Ga_2 have been grown by the Al-Ga self-flux method. The elements of europium, aluminum, and gallium were loaded into an alumina crucible in a ratio $\text{Eu}:\text{Al}:\text{Ga} = 1:8:4$ and subsequently sealed in a quartz-glass ampule under vacuum. The ampule was heated towards 1173 K, in order to obtain a homogenous solution. They were cooled at a rate of 2 K/hour to 873 K. At 873 K, the ampules were centrifuged to separate the single crystals from the flux. The stoichiometry of the crystals (i.e., $\text{Eu}:\text{Al}:\text{Ga} = 1:2:2$) has been confirmed using Energy-dispersive X-ray analysis (EDAX).

(B) Magnetic Properties

The temperature dependence of the magnetic susceptibility of EuAl_2Ga_2 was measured on a single crystal using a commercial superconducting quantum interference device (SQUID) magnetometer (MPMS 7, Quantum Design, USA). Data were obtained after cooling the samples under zero-field cooling (ZFC) and field cooling (FC) conditions. A magnetic field of 1 kOe was applied along the [001] direction of the sample.

(C) Single Crystal X-ray Diffraction (SXR)

Temperature-dependent SXR was carried out at beamline P24 of the synchrotron PETRA-III at DESY in Hamburg. A good-quality single crystal of EuAl_2Ga_2 was selected,

with dimensions of 0.09mm × 0.055mm × 0.018mm. The SXRD was measured at a Eulerian diffractometer at temperatures down to 18 K using a CRYOCOOL open-flow helium gas cryostat. A Pilatus 1M- CdTe detector was used for data collection. Synchrotron radiation of wavelength 0.5000 Å was used for the experiment. Different runs employed different attenuators in the monochromatised beam, of filter factors of 1, 1.4804 and 10.5263. SXRD data sets were measured for temperatures of 298 K and 85 K (tetragonal phase) and of 35, 30 and 18 K (CDW phase). Each run of the data collection contained 3640 frames of $\Delta\phi = 0.1$ deg and was repeated ten times. These data were binned to a data set of 364 frames of 1° of rotation and 10 sec exposure time per frame, using the programs *addrunscbf* and *combcbf* [40]. A single run at 298 K was recorded at 110 mm crystal-to-detector distance. Two runs were needed at 35, 30, and 18 K, with and without a 2θ offset, for a 260 mm crystal to detector distance. An improved spatial resolution was achieved at 35, 30 and 18 K through a crystal-to-detector distance of 270 mm. A similar resolution of the SXRD data then required runs with offsets of 0 and 25 deg in 2θ .

CrysAlis Pro [41] makes an unwarp image that is based on all of the measured scattering, including scattering between the Bragg reflections (**Figure 2**). The EVAL15 [42] software suite was used for data processing of the binned SXRD data. The two runs with different offsets in 2θ were integrated separately for each of the data measured at 35K, 30 K and 18 K. They were combined by the module ANY of EVAL15. An outlier rejection was based on tetragonal $4/mmm$ and orthorhombic mmm Laue classes. Absorption correction and scaling were performed in *SADABS* [43] with Laue symmetries $4/mmm$ for all five data sets and mmm for the data measured at 35, 30 and 18 K.

The resulting reflection files were imported into JANA2020 [44] for structure solution and refinement. The Laue symmetry $4/mmm$ and mmm is used for the periodic and CDW phases of EuAl_2Ga_2 . We have used the superspace approach to index and integrate the incommensurately modulated data to solve the crystal structure in the CDW phase [12,45]. The crystal structure is drawn using the program VESTA [46].

Results and discussion:

(A) Periodic Structure and Magnetic Properties

SXRD data at 298 K and 85 K confirmed the BaAl_4 structure type with space group $I4/mmm$ [Table 1, **Figure 1(a)**]. In this structure, the Eu^{2+} ions form a square layer in the ab

plane. Neighboring Eu layers are translated by (0.5, 0.5, 0.5) due to the *I*-centering. The Al and Ga atoms lie between neighboring Eu layers and are ordered on Wyckoff positions 4d and 4e, respectively. The refined composition (EuAl_{2.023(21)}Ga_{1.977}) is close to the nominal composition EuAl₂Ga₂. Since Ga thus substitutes for the Al₂ atom of EuAl₄, the atomic sites in EuAl₂Ga₂ are designated as Eu1, Al1, and Ga2. The substitution of Al by Ga results in a reduced volume of EuAl₂Ga₂ as compared to EuAl₄ [18] and SrAl₄ [39].

Previous studies have found that Ga-doped Eu(Al_{1-x}Ga_x)₄ compounds exhibit antiferromagnetic transitions below 25 K [23]. **Figure 1(b-d)** shows the temperature-dependent zero-field cooled (ZFC) and field cooled (FC) *dc* magnetization of EuAl₂Ga₂ in the temperature range of 2 K – 100 K, and the presence of 1k Oe magnetic field applied parallel to the *c*-axis. The magnetization curve shows an antiferromagnetic nature of the sample where the FC magnetization follows the trend of ZFC magnetization. The inverse susceptibility curve obtained from the ZFC magnetization is shown in **Figure 1(c)**. A Curie-Weiss fit to the paramagnetic region (55–100 K) resulted in a positive Curie-Weiss temperature that indicates dominant ferromagnetic interactions, despite the antiferromagnetic ordering at lower temperatures. The effective magnetic moment (μ_{eff}) for EuAl₂Ga₂ is 7.917 μ_{B} , which is close to the theoretical of 7.937 μ_{B} .

Neutron diffraction studies have provided the incommensurate helical and cycloidal magnetic phases of antiferromagnetic EuAl₂Ga₂ below T_{N} [22]. Multiple magnetic transitions can be identified by the dips in the first derivative of magnetization (*dM/dT*) curve. These transition temperatures are $T_{\text{N}1} = 21.4$ K, $T_{\text{N}2} = 15.78$ K, $T_{\text{N}3} = 11.02$ K, and $T_{\text{N}4} = 7.45$ K, for a magnetic field of 1 kOe applied parallel to the *c* axis, as shown in **Figure 1(d)**. These transition temperatures are very close to those reported by *Stavinoha et al.* [23].

(B) Temperature-dependent CDW structure

The first-order, CDW phase transition of EuAl₂Ga₂ has been reported to occur at $T_{\text{CDW}} \approx 51$ K experiments [22,23]. **Figure 2** shows parts of (*h* 0 *l*) sections of reciprocal space, reconstructed from SXRD data at four different temperatures. First-order satellites are clearly visible along *c** at 35 K, 30 K and 18 K. They represent the incommensurately modulated CDW with wave vectors (0, 0, 0.1141(2)) at 35 K, (0, 0, 0.1139 (2)) at 30 K and (0, 0, 0.1126

(4)) at 18 K. The value of the incommensurate component decreases with decreasing temperature. Higher-order satellites have not been observed.

We have observed that EuAl_2Ga_2 preserves tetragonal $I4/mmm$ symmetry as symmetry of the basic structure in the CDW state, as it was also found for EuAl_4 and SrAl_4 [18, 40]. The incommensurate CDW phase of EuAl_4 has the orthorhombic symmetry $Fmmm(00\gamma)s00$ with modulation wave vector $\mathbf{q} = (0, 0, 0.1781(3))$ at 70 K and $\mathbf{q} = (0, 0, 0.1741(2))$ at 20 K [18]. For the CDW phase of EuAl_2Ga_2 , the present SXR data indicate symmetry according to the superspace group $Immm(00\gamma)s00$, as detailed below. This finding is in line with the results of Resonant Inelastic X-ray scattering (RIXS), which indicated the loss of the fourfold symmetry in the CDW state of EuAl_2Ga_2 [38].

In order to establish the crystal structure and symmetry of the CDW state of EuAl_2Ga_2 , the SXR data were initially processed according to $4/mmm$ point symmetry. Averaging in JANA2020 showed that these SXR data fulfil $4/mmm$ point symmetry very well according to the observed values of R_{int} (see **Table 2**). However, structure refinements at 35 K, 30 K and 18 K employing a tetragonal superspace group lead to high values for R_{F} (satellite) (Table 2 and Tables S4 and S5). Exception is the superspace group $I422(00\gamma)q00$, but R values attained with this non-centrosymmetric superspace group are still significantly higher than those for the orthorhombic choices. Therefore, these results confirm that the CDW phase doesn't have tetragonal symmetry. Secondly, structure models were employed with superspace groups based on orthorhombic subgroups of $I4/mmm$. SXR data processed in $4/mmm$ symmetry imply two orthorhombic domains with twin fractions 0.5 : 0.5. Structure refinements then led to comparable R values for orthorhombic superspace groups $Fmmm(00\gamma)s00$ and $Immm(00\gamma)s00$ (**Table 2**).

In a second approach, structure refinements of models with $Fmmm(00\gamma)s00$ and $Immm(00\gamma)s00$ symmetries have been performed against the SXR data processed according to the respective orthorhombic point symmetries $Fmmm$ and $Immm$. Here, R values indicate a better fit for $Immm(00\gamma)s00$ than for $Fmmm(00\gamma)s00$ for all the temperatures (**Table 2**). Volumes for the twin domains were refined and they deviate significantly from 0.5 : 0.5 for the structure in $Immm(00\gamma)s00$ (**Table 1**). **Table 3** provides the basic-structure coordinates of EuAl_2Ga_2 at 298 K and 85 K with $I4/mmm$ symmetry, and at 35 K, 30 K and 18 K with orthorhombic $Immm(00\gamma)s00$ symmetry. The basic structure of EuAl_2Ga_2 retains tetragonal symmetry at all temperatures, since the z -coordinate of Al1 does not deviate significantly from

0.25. Details on the structure model with $Fmmm(00\gamma)s00$ symmetry are proved in **Tables S1–S3** in the Supplementary Material.

Recently, we have found for $SrAl_4$ that a non-centrosymmetric structure with symmetry $F222(00\gamma)00s$ give a better fit to the SXRD data than its supergroup $Fmmm(00\gamma)s00$ [36,39]. Main argument was a better fit to the second-order satellites for the non-centrosymmetric model [39]. For $EuAl_4$, the SXRD data set did not contain second-order satellites, and the centrosymmetric and non-centrosymmetric models could not be distinguished [18,39]. Presently, without second-order satellites for $EuAl_2Ga_2$, non-centrosymmetric superspace groups do lead to better fits to the data than the superspace group $Immm(00\gamma)s00$ (**Table 2**). Furthermore, refinements are unstable for superspace groups based on point symmetry 222, thus indicating dependencies between the parameters. A complete list of non-centrosymmetric space groups for 18 K is shown in **Table S4** of Supplementary Material. In conclusion, the present SXRD data lead to a centrosymmetric structure model for the CDW state of $EuAl_2Ga_2$, which has orthorhombic symmetry $Immm(00\gamma)s00$.

(C) Thermal expansion

The present data reveal negative thermal expansion (NTE) below the CDW transition (**Table 1; Figure 3**). It has been shown that NTE can be enhanced by substituting Al, Ga, and Cr in various intermetallics [47], which also enhances the magnetic transition temperature [48]. This general feature thus explains the present observation of NTE of $EuAl_2Ga_2$. NTE has been found in other RT_2X_2 compounds like $YbMn_2Ge_2$ compound over a wide temperature range [49]. The NTE ($\alpha_V = \frac{1}{V}(\frac{dV}{dT})$) at the temperature difference of 35K-30K and 30K-18K are $-2.06 \times 10^{-3} K^{-1}$ and $-2.17 \times 10^{-4} K^{-1}$ observed with space group $Immm(00\gamma)s00$.

(D) Location of the CDW

Structural parameters, such as atomic displacements, atomic distances and bond angles, can be evaluated as a function of the phase t of the modulation wave. Such t -plots are useful for analyzing the correlated variations of different parameters, e.g. of the atomic environments. The displacement modulation is described by a modulation function for each atom of the form [12],

$$u_{\alpha}(\bar{x}_{s4}) = \sum_n \{A_{\alpha,n} \sin(2n\pi \bar{x}_{s4}) + B_{\alpha,n} \cos(2n\pi \bar{x}_{s4})\} \quad (1)$$

where $n = 1$ due to first order harmonics and $\alpha = x, y, z$. The fourth superspace coordinate for the j^{th} atom can be represented as, $\bar{x}_{s4}(j) = t + \mathbf{q} \cdot \bar{\mathbf{x}}(j)$ where t is the initial phase of modulation and $\bar{\mathbf{x}}(j)$ is the position of the j^{th} atom in the periodic basic structure [12]. The observed amplitudes for displacement modulation show that atoms have displacements (u_x) along the x direction and zero displacements u_y along y and u_z along z for the structure models with superspace group $Immm(00\gamma)s00$ [Table 4 and Figure 4 (a-c)]. The non-zero modulation amplitudes for all three atoms contribute to CDW order in the material. However, the Eu1 atom is elastically coupled to Al1 and Ga2 atoms, having the *sine* component of modulation function, whereas Al1 and Ga2 have both periodic components of *sine* and *cosine* waves along the x direction. Displacement modulation for all the atoms is a transverse wave.

To understand how Al1 and Ga2 atoms contribute to CDW ordering in the material, we consider the shortest interatomic distances, which are Ga2–Ga2, Ga2–Al1 and Al1–Al1 distances. t -plots of these interatomic distances show that the largest modulation is found for the Al1–Al1 distances at all three temperatures (Figures 5 and 6; Figures S1–S3). This finding suggests that the CDW resides on the Al atoms, like for EuAl₄ [18]. The different symmetries of the CDWs in EuAl₂Ga₂ and EuAl₄ [18] can be attributed to the presence of Ga in EuAl₂Ga₂.

Conclusions

Like EuGa₄, EuAl₄ and SrAl₄; EuAl₂Ga₂ has the BaAl₄ structure type with tetragonal symmetry $I4/mmm$ at room temperature. SXR D shows the presence of satellite reflections along \mathbf{c}^* at temperatures below $T_{\text{CDW}} = 51$ K. The incommensurately modulated CDW crystal structure of EuAl₂Ga₂ was found to possess symmetry according to the superspace group $Immm(00\gamma)s00$. This is different from EuAl₄ that has superspace symmetry $Fmmm(00\gamma)s00$ for its CDW state, and it is different from EuGa₄, which does not develop a CDW at ambient pressure. The different symmetries of the CDW states of EuAl₄ and EuAl₂Ga₂ might thus be explained by the effects of Ga substitution in the latter compound. In this respect, it should be noted that both structure models, $Fmmm(00\gamma)s00$ and $Immm(00\gamma)s00$, lead to a large variation of the Al1–Al1 contact distance as principal effect of the modulation. Either model thus explains the presence of the CDW on the Al1 atoms.

We have found negative thermal expansion (NTE) below T_{CDW} . The NTE effect can be rationalized as the result of Ga substitution into this intermetallic material [45].

Acknowledgement:

We thank Kerstin Küspert and Franz Fischer for technical assistance with the experiments. We acknowledge DESY (Hamburg, Germany), a member of the Helmholtz Association HGF, for the provision of experimental facilities. Parts of this research were carried out at PETRA-III, and we would like to thank Heiko Schulz-Ritter for assistance in using beamline P24. Beamtime was allocated for proposal I-20211203.

Reference:

- [1] F. Giustino, J. H. Lee, F. Trier, M. Bibes, S. M. Winter, R. Valentí, Y.-W. Son, L. Taillefer, C. Heil, A. I. Figueroa, B. Plaçais, Q. Wu, O. V. Yazyev, E. P. A. M. Bakkers, J. Nygård, P. Forn-Díaz, S. De Franceschi, J. W. McIver, L. E. F. F. Torres, T. Low, A. Kumar, R. Galceran, S. O. Valenzuela, M. V. Costache, A. Manchon, E.-A. Kim, G. R. Schleder, A. Fazzio, and S. Roche, *The 2021 Quantum Materials Roadmap*, Journal of Physics: Materials **3**, 042006 (2020).
- [2] D. N. Basov, R. D. Averitt, and D. Hsieh, *Towards Properties on Demand in Quantum Materials*, Nature Materials **16**, 1077 (2017).
- [3] N. Kumar, S. N. Guin, K. Manna, C. Shekhar, and C. Felser, *Topological Quantum Materials from the Viewpoint of Chemistry*, Chemical Reviews **121**, 2780 (2021).
- [4] B. A. Bernevig, C. Felser, and H. Beidenkopf, *Progress and Prospects in Magnetic Topological Materials*, Nature **603**, 41 (2022).
- [5] S. Klemenz, A. K. Hay, S. M. L. Teicher, A. Topp, J. Cano, and L. M. Schoop, *The Role of Delocalized Chemical Bonding in Square-Net-Based Topological Semimetals*, Journal of the American Chemical Society **142**, 6350 (2020).
- [6] M. Shatruk, *ThCr₂Si₂ Structure Type: The “Perovskite” of Intermetallics*, Journal of Solid State Chemistry **272**, 198 (2019).
- [7] S. D. Ramarao, A. K. Singh, U. Subbarao, and S. C. Peter, *An Overview on the Structural Diversity of Europium Based Ternary Intermetallics*, Journal of Solid State Chemistry **281**, 121048 (2020).
- [8] J. Bouaziz, E. Mendive-Tapia, S. Blügel, and J. B. Staunton, *Fermi-Surface Origin of Skyrmion Lattices in Centrosymmetric Rare-Earth Intermetallics*, Physical Review Letters **128**, 157206 (2022).
- [9] J. P. Pouget and E. Canadell, *Structural Approach to Charge Density Waves in Low-Dimensional Systems: Electronic Instability and Chemical Bonding*, Reports on Progress in Physics **87**, 026501 (2024).
- [10] X. Zhu, Y. Cao, J. Zhang, E. W. Plummer, and J. Guo, *Classification of Charge Density Waves Based on Their Nature*, Proceedings of the National Academy of Sciences of the United States of America **112**, 2367 (2015).
- [11] X. Zhu, J. Guo, J. Zhang, and E. W. Plummer, *Misconceptions Associated with the Origin of Charge Density Waves*, Advances in Physics: X **2**, 622 (2017).
- [12] S. van Smaalen, *Incommensurate Crystallography* (Oxford University Press, 2007).
- [13] W. R. Meier, J. R. Torres, R. P. Hermann, J. Zhao, B. Lavina, B. C. Sales, and A. F. May, *Thermodynamic Insights into the Intricate Magnetic Phase Diagram of EuAl₄*, Physical Review B **106**, 094421 (2022).
- [14] A. Nakamura, T. Uejo, H. Harima, S. Araki, T. C. Kobayashi, M. Nakashima, Y. Amako, M. Hedo, T. Nakama, and Y. Onuki, *Characteristic Fermi Surfaces and Charge Density Wave in SrAl₄ and Related Compounds with the BaAl₄-Type Tetragonal Structure*, Journal of Alloys and Compounds **654**, 290 (2016).
- [15] S. Ramakrishnan, J. Bao, C. Eisele, B. Patra, M. Nohara, B. Bag, L. Noohinejad, M.

- Tolkiehn, C. Paulmann, A. M. Schaller, T. Rekiş, S. R. Kotla, A. Schönleber, A. Thamizhavel, B. Singh, S. Ramakrishnan, and S. van Smaalen, *Coupling between Charge Density Wave Ordering and Magnetism in Ho₂Ir₃Si₅*, *Chemistry of Materials* **35**, 1980 (2023).
- [16] S. Ramakrishnan, A. Schönleber, T. Rekiş, N. Van Well, L. Noohinejad, S. Van Smaalen, M. Tolkiehn, C. Paulmann, B. Bag, A. Thamizhavel, D. Pal, and S. Ramakrishnan, *Unusual Charge Density Wave Transition and Absence of Magnetic Ordering in Er₂Ir₃Si₅*, *Physical Review B* **101**, 060101 (2020).
- [17] S. Shimomura, H. Murao, S. Tsutsui, H. Nakao, A. Nakamura, M. Hedo, T. Nakama, and Y. Ōnuki, *Lattice Modulation and Structural Phase Transition in the Antiferromagnet EUAL₄*, *Journal of the Physical Society of Japan* **88**, (2019).
- [18] S. Ramakrishnan, S. R. Kotla, T. Rekiş, J. K. Bao, C. Eisele, L. Noohinejad, M. Tolkiehn, C. Paulmann, B. Singh, R. Verma, B. Bag, R. Kulkarni, A. Thamizhavel, B. Singh, S. Ramakrishnan, and S. Van Smaalen, *Orthorhombic Charge Density Wave on the Tetragonal Lattice of EuAl₄*, *IUCrJ* **9**, 378 (2022).
- [19] M. Gen, R. Takagi, Y. Watanabe, S. Kitou, H. Sagayama, N. Matsuyama, Y. Kohama, A. Ikeda, Y. Ōnuki, T. Kurumaji, T. H. Arima, and S. Seki, *Rhombic Skyrmion Lattice Coupled with Orthorhombic Structural Distortion in EuAl₄*, *Physical Review B* **107**, L020410 (2023).
- [20] G. J. Miller, F. Li, and H. F. Franzen, *The Structural Phase Transition in CaAl₄: A Concerted Application of Landau Theory and Energy Band Theory*, *Journal of the American Chemical Society* **115**, 3739 (1993).
- [21] S. Engel, E. C. J. Gieβelmann, L. E. Schank, G. Heymann, K. Brix, R. Kautenburger, H. P. Beck, and O. Janka, *Theoretical and 27Al NMR Spectroscopic Investigations of Binary Intermetallic Alkaline-Earth Aluminides*, *Inorganic Chemistry* **62**, 4260 (2023).
- [22] J. M. Moya, S. Lei, E. M. Clements, C. S. Kengle, S. Sun, K. Allen, Q. Li, Y. Y. Peng, A. A. Husain, M. Mitranò, M. J. Krogstad, R. Osborn, A. B. Puthirath, S. Chi, L. Debeer-Schmitt, J. Gaudet, P. Abbamonte, J. W. Lynn, and E. Morosan, *Incommensurate Magnetic Orders and Topological Hall Effect in the Square-Net Centrosymmetric EuGa₂Al₂ System*, *Physical Review Materials* **6**, 074201 (2022).
- [23] M. Stavinoha, J. A. Cooley, S. G. Minasian, T. M. McQueen, S. M. Kauzlarich, C. L. Huang, and E. Morosan, *Charge Density Wave Behavior and Order-Disorder in the Antiferromagnetic Metallic Series Eu(Ga_{1-x}Al_x)₄*, *Physical Review B* **97**, 195146 (2018).
- [24] A. Nakamura, T. Uejo, F. Honda, T. Takeuchi, H. Harima, E. Yamamoto, Y. Haga, K. Matsubayashi, Y. Uwatoko, M. Hedo, T. Nakama, and Y. Ōnuki, *Transport and Magnetic Properties of EuAl₄ and EuGa₄*, *Journal of the Physical Society of Japan* **84**, (2015).
- [25] R. Takagi, N. Matsuyama, V. Ukleev, L. Yu, J. S. White, S. Francoual, J. R. L. Mardegan, S. Hayami, H. Saito, K. Kaneko, K. Ohishi, Y. Ōnuki, T. hisa Arima, Y. Tokura, T. Nakajima, and S. Seki, *Square and Rhombic Lattices of Magnetic Skyrmions in a Centrosymmetric Binary Compound*, *Nature Communications* **13**, 1 (2022).
- [26] W. Wang, Y. Zhang, G. Xu, L. Peng, B. Ding, Y. Wang, Z. Hou, X. Zhang, X. Li, E. Liu, S. Wang, J. Cai, F. Wang, J. Li, F. Hu, G. Wu, B. Shen, and X. X. Zhang, *A*

- Centrosymmetric Hexagonal Magnet with Superstable Biskyrmion Magnetic Nanodomains in a Wide Temperature Range of 100–340 K*, *Advanced Materials* **28**, 6887 (2016).
- [27] T. Kurumaji, T. Nakajima, M. Hirschberger, A. Kikkawa, Y. Yamasaki, H. Sagayama, H. Nakao, Y. Taguchi, T. hisa Arima, and Y. Tokura, *Skyrmion Lattice with a Giant Topological Hall Effect in a Frustrated Triangular-Lattice Magnet*, *Science* **365**, 914 (2019).
- [28] G. D. A. Wood, D. D. Khalyavin, D. A. Mayoh, J. Bouaziz, A. E. Hall, S. J. R. Holt, F. Orlandi, P. Manuel, S. Blügel, J. B. Staunton, O. A. Petrenko, M. R. Lees, and G. Balakrishnan, *Double- Q Ground State with Topological Charge Stripes in the Centrosymmetric Skyrmion Candidate $GdRu_2Si_2$* , *Physical Review B* **107**, L180402 (2023).
- [29] M. Hirschberger, T. Nakajima, S. Gao, L. Peng, A. Kikkawa, T. Kurumaji, M. Kriener, Y. Yamasaki, H. Sagayama, H. Nakao, K. Ohishi, K. Kakurai, Y. Taguchi, X. Yu, T. hisa Arima, and Y. Tokura, *Skyrmion Phase and Competing Magnetic Orders on a Breathing Kagomé Lattice*, *Nature Communications* **10**, 1 (2019).
- [30] M. Merz, L. Wang, T. Wolf, P. Nagel, C. Meingast, and S. Schuppler, *Rotational Symmetry Breaking at the Incommensurate Charge-Density-Wave Transition in $Ba(Ni,Co)_2(As,P)_2$: Possible Nematic Phase Induced by Charge/Orbital Fluctuations*, *Physical Review B* **104**, 184509 (2021).
- [31] Y. Yao, R. Willa, T. Lacmann, S.-M. Souliou, M. Frchet, K. Willa, M. Merz, F. Weber, C. Meingast, R. Heid, A.-A. Haghighirad, J. Schmalian, and M. Le Tacon, *An Electronic Nematic Liquid in $BaNi_2As_2$* , *Nature Communications* **13**, 4535 (2022).
- [32] M. Frchet, P. Wiecki, T. Lacmann, S. M. Souliou, K. Willa, C. Meingast, M. Merz, A. A. Haghighirad, M. Le Tacon, and A. E. Böhmer, *Elastoresistivity in the Incommensurate Charge Density Wave Phase of $BaNi_2(As_{1-x}Px)_2$* , *Npj Quantum Materials* **7**, 1 (2022).
- [33] L. Kautzsch, B. R. Ortiz, K. Mallayya, J. Plumb, G. Pokharel, J. P. C. Ruff, Z. Islam, E. A. Kim, R. Seshadri, and S. D. Wilson, *Structural Evolution of the Kagome Superconductors $A V_3Sb_5$ ($A = K, Rb, \text{ and } Cs$) through Charge Density Wave Order*, *Physical Review Materials* **7**, 024806 (2023).
- [34] C. Shi, Y. Liu, B. B. Maity, Q. Wang, S. R. Kotla, S. Ramakrishnan, C. Eisele, H. Agarwal, L. Noohinejad, Q. Tao, B. Kang, Z. Lou, X. Yang, Y. Qi, X. Lin, Z.-A. Xu, A. Thamizhavel, G.-H. Cao, S. van Smaalen, S. Cao, and J.-K. Bao, *Annealing-Induced Long-Range Charge Density Wave Order in Magnetic Kagome $FeGe$: Fluctuations and Disordered Structure*, *ArXiv: 2308.09034* (2023).
- [35] C. Shi, H. Deng, S. R. Kotla, Y. Liu, S. Ramakrishnan, C. Eisele, H. Agarwal, L. Noohinejad, J.-Y. Liu, T. Yang, G. Liu, B. B. Maity, Q. Wang, Z. Lin, B. Kang, W. Yang, Y. Li, Z. Yang, Y. Li, Y. Qi, A. Thamizhavel, W. Ren, G.-H. Cao, J.-X. Yin, S. van Smaalen, S. Cao, and J.-K. Bao, *Charge Density Wave without Long-Range Structural Modulation in Canted Antiferromagnetic Kagome $FeGe$* , *ArXiv: 2404.00996* (2024).
- [36] H. Ni, W. R. Meier, H. Miao, A. J. May, B. C. Sales, J. Zuo, and M. Chi, *Real-Space Visualization of Charge Density Wave Induced Local Inversion-Symmetry Breaking in*

- a Skyrmion Magnet*, ArXiv: 2311.17682 (2023).
- [37] A. N. Korshunov, A. S. Sukhanov, S. Gebel, M. S. Pavlovskii, N. D. Andriushin, Y. Gao, J. M. Moya, E. Morosan, and M. C. Rahn, *Phonon Softening and Atomic Modulations in EuAl₄*, *Physical Review B* **110**, 045102 (2024).
- [38] A. M. Vibhakar, D. D. Khalyavin, J. M. Moya, P. Manuel, F. Orlandi, S. Lei, E. Morosan, and A. Bombardi, *Competing Charge and Magnetic Order in the Candidate Centrosymmetric Skyrmion Host EuGa₂Al₂*, *Physical Review B* **108**, (2023).
- [39] S. Ramakrishnan, S. R. Kotla, H. Pi, B. B. Maity, J. Chen, J. K. Bao, Z. Guo, M. Kado, H. Agarwal, C. Eisele, M. Nohara, L. Noohinejad, H. Weng, S. Ramakrishnan, A. Thamizhavel, and S. Van Smaalen, *Noncentrosymmetric, Transverse Structural Modulation in SrAl₄, and Elucidation of Its Origin in the BaAl₄ Family of Compounds*, *Physical Review Research* **6**, 023277 (2024).
- [40] C. Paulmann and M. Tolkehn, *Binning Software: Addruncbf, Combcbf, for Avargaing Fine Slicing Frames and Dead Time Correction Pilatus and Lambda Detector*, PETRA III, DESY (2023).
- [41] *Crysalis Pro: Data Collection and Data Reduction GUI, Version 171.43.131a*, Rigaku Oxford Diffraction (2024).
- [42] A. M. M. Schreurs, X. Xian, and L. M. J. Kroon-Batenburg, *EVAL15: A Diffraction Data Integration Method Based on Ab Initio Predicted Profiles*, *Journal of Applied Crystallography* **43**, 70 (2010).
- [43] L. Krause, R. Herbst-Irmer, G. M. Sheldrick, and D. Stalke, *Comparison of Silver and Molybdenum Microfocus X-Ray Sources for Single-Crystal Structure Determination*, *Journal of Applied Crystallography* **48**, 3 (2015).
- [44] V. Petříček, L. Palatinus, J. Plášil, and M. Dušek, *Jana2020 – a New Version of the Crystallographic Computing System Jana*, *Zeitschrift Für Kristallographie - Crystalline Materials* **238**, 271 (2023).
- [45] A. Janner and T. Janssen, *Symmetry of Incommensurate Crystal Phases. I. Commensurate Basic Structures*, *Acta Crystallographica Section A* **36**, 399 (1980).
- [46] K. Momma and F. Izumi, *VESTA: A Three-Dimensional Visualization System for Electronic and Structural Analysis*, *Journal of Applied Crystallography* **41**, 653 (2008).
- [47] K. Takenaka, *Negative Thermal Expansion Materials: Technological Key for Control of Thermal Expansion*, *Science and Technology of Advanced Materials* **13**, 013001 (2012).
- [48] J. Chen, L. Hu, J. Deng, and X. Xing, *Negative Thermal Expansion in Functional Materials: Controllable Thermal Expansion by Chemical Modifications*, *Chemical Society Reviews* **44**, 3522 (2015).
- [49] Y. Qiao, Y. Song, A. Sanson, L. Fan, Q. Sun, S. Hu, L. He, H. Zhang, X. Xing, and J. Chen, *Negative Thermal Expansion in YbMn₂Ge₂ Induced by the Dual Effect of Magnetism and Valence Transition*, *Npj Quantum Materials* **6**, 1 (2021).

Table 1. Crystallographic data of EuAl_2Ga_2 at temperatures of 298 K, 85 K, 35 K, 30 K and 18 K. The criterion of observability is $I > 3 \sigma(I)$. a, b, c are the lattice parameters, V is the volume of the unit cell of the basic structure, and q_z is the z component of the modulation wave vector. D is the detector distance; twvol is twin volume.

Temperature	298 K	85 K	35 K	30 K	18 K
Crystal System	Tetragonal	Tetragonal	Orthorhombic	Orthorhombic	Orthorhombic
Space Group	<i>I4/mmm</i>	<i>I4/mmm</i>	<i>Immm(00γ)s00</i>	<i>Immm(00γ)s00</i>	<i>Immm(00γ)s00</i>
No.	139	139	71.1.12.2	71.1.12.2	71.1.12.2
Laue symmetry	<i>4/mmm</i>	<i>4/mmm</i>	<i>mmm</i>	<i>mmm</i>	<i>mmm</i>
a (Å)	4.3389(38)	4.33410(16)	4.29366(14)	4.30768(14)	4.31351(25)
b (Å)	4.3389	4.33410	4.29677(10)	4.31402(13)	4.31411(19)
c (Å)	10.9674(77)	10.95703(47)	10.86970(25)	10.90222(31)	10.91571(54)
V (Å ³)	206.47(41)	205.822(20)	200.534(9)	202.601(12)	203.130(20)
q_z	-	-	0.1142(2)	0.1139 (2)	0.1126(4)
D (mm)	110	260	260	260	260
Filter factor	10.5263	10.5263	1.4804+10.5263	0+10.5263	0+10.5263
2 θ offset	0	0, 25	0, 25	0, 25	0, 25
$[\text{Sin}(\theta)/\lambda]_{\text{max}} \text{Å}^{-1}$	0.690825	0.730126	0.734924	0.732604	0.731724
No. of Reflections					
Main (obs/all)	105/108	119/122	153/174	142/161	148/168
Satellites (obs/all)	-	-	179/333	140/331	150/332
R _{int} (obs/all) %	3.67/3.67	1.78/1.78	2.97/3.03	2.33/2.41	2.17/2.22
No. of parameters	9	9	16	16	16
R _F (all) %	1.53	1.60	3.47	3.23	2.50
_w R _F ² (all)%	1.99	2.12	4.67	3.74	2.85
R _F (main) %	1.53	1.59	2.56	2.63	2.07
R _F (sat) %	-	-	7.84	6.44	4.70
GOF (obs/all)	1.64/1.61	1.66/1.64	1.71/1.41	1.31/1.01	0.98/0.77
twvol1/twvol2	-	-	0.386(8)/0.614	0.419(9)/0.581	0.447(6)/0.552

Table 2. R values (%) of different structure models on the basis of different centrosymmetric and non-centrosymmetric superspace groups for SXRD data at 35 K, 30 K, 18 K.

Superspace group	averaging	R _{int}	R _F (all)	R _F (Main)	R _F (Satellite)	wR _F ² (all)	Number of Reflections (Main / Satellite)	Parameter
Temperature = 35 K								
<i>I4/mmm(00γ)000</i>	<i>4/mmm</i>	3.28	12.73	3.12	59.91	19.92	99/105	13
<i>Fmmm(00γ)s00</i>	<i>4/mmm</i>	3.28	3.02	1.91	8.46	3.56	99/105	14
<i>Immm(00γ)s00</i>	<i>4/mmm</i>	3.28	2.98	1.90	8.30	3.58	99/105	15
<i>Fmmm(00γ)s00</i>	<i>mmm</i>	2.77	3.59	2.40	9.57	4.39	147/161	15
<i>F222(00γ)00s</i>	<i>mmm</i>	2.77	3.55	2.39	9.38	4.36	147/161	19
<i>Immm(00γ)s00</i>	<i>mmm</i>	2.97	3.47	2.56	7.84	4.67	153/179	16
<i>I222(00γ)00s</i>	<i>mmm</i>	2.97	3.46	2.56	7.76	4.66	153/179	20
<i>I422(00γ)q00</i>	<i>mmm</i>	2.97	3.82	2.67	9.36	5.47	153/179	14
Temperature = 30 K								
<i>I4/mmm(00γ)000</i>	<i>4/mmm</i>	2.88	15.31	4.75	64.98	23.98	92/105	13
<i>Fmmm(00γ)s00</i>	<i>4/mmm</i>	2.88	2.77	1.96	6.53	3.31	92/105	14
<i>Immm(00γ)s00</i>	<i>4/mmm</i>	2.88	2.75	1.97	6.43	3.35	92/105	15
<i>Fmmm(00γ)s00</i>	<i>mmm</i>	2.89	3.82	2.82	8.60	4.66	148/162	15
<i>F222(00γ)00s</i>	<i>mmm</i>	2.89	3.76	2.80	8.46	4.63	148/162	19
<i>Immm(00γ)s00</i>	<i>mmm</i>	2.33	3.24	2.63	6.45	3.74	142/140	16
<i>I222(00γ)00s</i>	<i>mmm</i>	2.33	3.22	2.63	6.37	3.74	142/140	20
<i>I422(00γ)q00</i>	<i>mmm</i>	2.33	3.39	2.64	7.39	3.99	142/140	14
Temperature = 18 K								
<i>I4/mmm(00γ)000</i>	<i>4/mmm</i>	2.69	12.66	2.88	59.68	19.70	97/105	13
<i>Fmmm(00γ)s00</i>	<i>4/mmm</i>	2.69	2.13	1.56	4.85	2.45	97/105	14
<i>Immm(00γ)s00</i>	<i>4/mmm</i>	2.69	2.13	1.56	4.85	2.47	97/105	15
<i>Fmmm(00γ)s00</i>	<i>mmm</i>	2.60	2.91	2.27	6.12	3.31	151/150	15
<i>F222(00γ)00s</i>	<i>mmm</i>	2.60	2.87	2.27	5.92	3.28	151/150	19
<i>Immm(00γ)s00</i>	<i>mmm</i>	2.17	2.50	2.07	4.71	2.86	148/150	16
<i>I222(00γ)00s</i>	<i>mmm</i>	2.17	2.49	2.07	4.64	2.85	148/150	20
<i>I422(00g)q00</i>	<i>mmm</i>	2.17	2.59	2.11	5.05	3.01	148/150	14

Table 3. Atomic coordinates of EuAl₂Ga₂ as obtained from structure refinements against SXR data at 298 K and 85 K (crystal structure), and at 35 K, 30 K, and 18 K (basic structure).

Atoms	x	y	z	U11	U22	U33	U12	U13	U23	Ueq
<i>298 K (I4/mmm)</i>										
Eu1	0	0	0	0.0087(3)	0.0087(3)	0.0096(3)	0	0	0	0.0090(1)
Al1	0	0.5	0.25	0.0085(5)	0.0085(5)	0.0067(7)	0	0	0	0.0079(3)
Ga2	0	0	0.38561(6)	0.0112(3)	0.0112(3)	0.0073(4)	0	0	0	0.0073(4)
<i>85 K (I4/mmm)</i>										
Eu1	0	0	0	0.0030(2)	0.0030(2)	0.0039(3)	0	0	0	0.0033(1)
Al1	0	0.5	0.25	0.0030(5)	0.0030(5)	0.0031(7)	0	0	0	0.0030(3)
Ga2	0	0	0.38564(6)	0.0045(3)	0.0045(3)	0.0041(3)	0	0	0	0.0043(1)
<i>35 K (Immm(00γ)s00)</i>										
Eu1	0	0	0	0.0032(3)	0.0032(3)	0.0034(4)	0	0	0	0.0033(2)
Al1	0	0.5	0.2514(8)	0.0030(10)	0.0030(10)	0.0011(14)	0	0	0	0.0024(5)
Ga2	0	0	0.38566(9)	0.0040(4)	0.0040(4)	0.0031(5)	0	0	0	0.0037(2)
<i>30 K (Immm(00γ)s00)</i>										
Eu1	0	0	0	0.0047(3)	0.0047(3)	0.0037(3)	0	0	0	0.00433(17)
Al1	0	0.5	0.2497(10)	0.0025(9)	0.0025(9)	0.0010(12)	0	0	0	0.0020(6)
Ga2	0	0	0.38562(8)	0.0059(4)	0.0059(4)	0.0032(4)	0	0	0	0.0050(2)
<i>18 K (Immm(00γ)s00)</i>										
Eu1	0	0	0	0.0031(2)	0.0031(2)	0.0019(2)	0	0	0	0.00271(12)
Al1	0	0.5	0.2486(7)	0.0025(6)	0.0025(6)	0.0001(8)	0	0	0	0.0017(4)
Ga2	0	0	0.38565(6)	0.0045(3)	0.0045(3)	0.0017(3)	0	0	0	0.00358(16)

Table 4. Amplitudes of the modulation functions of structure models for EuAl_2Ga_2 at 35 K, 30 K and 18 K, for the superspace group $Immm(00\gamma)s00$.

Atoms	$A_{1,x}$ a (Å)	$A_{1,y}$ b (Å)	$A_{1,z}$ c (Å)	$B_{1,x}$ a (Å)	$B_{1,y}$ b (Å)	$B_{1,z}$ c (Å)
35 K ($Immm(00\gamma)s00$)						
Eu1	0.07979(35)	0	0	0	0	0
Al1	0.07629(133)	0	0	-0.02742(155)	0	0
Ga2	0.07999(56)	0	0	0.02860(45)	0	0
30 K ($Immm(00\gamma)s00$)						
Eu1	0.07804(38)	0	0	0	0	0
Al1	0.07420(139)	0	0	-0.02489(170)	0	0
Ga2	0.07968(61)	0	0	0.02864(51)	0	0
18 K ($Immm(00\gamma)s00$)						
Eu1	0.07987(28)	0	0	0	0	0
Al1	0.07869(115)	0	0	-0.02435(132)	0	0
Ga2	0.07975(45)	0	0	0.02813(39)	0	0

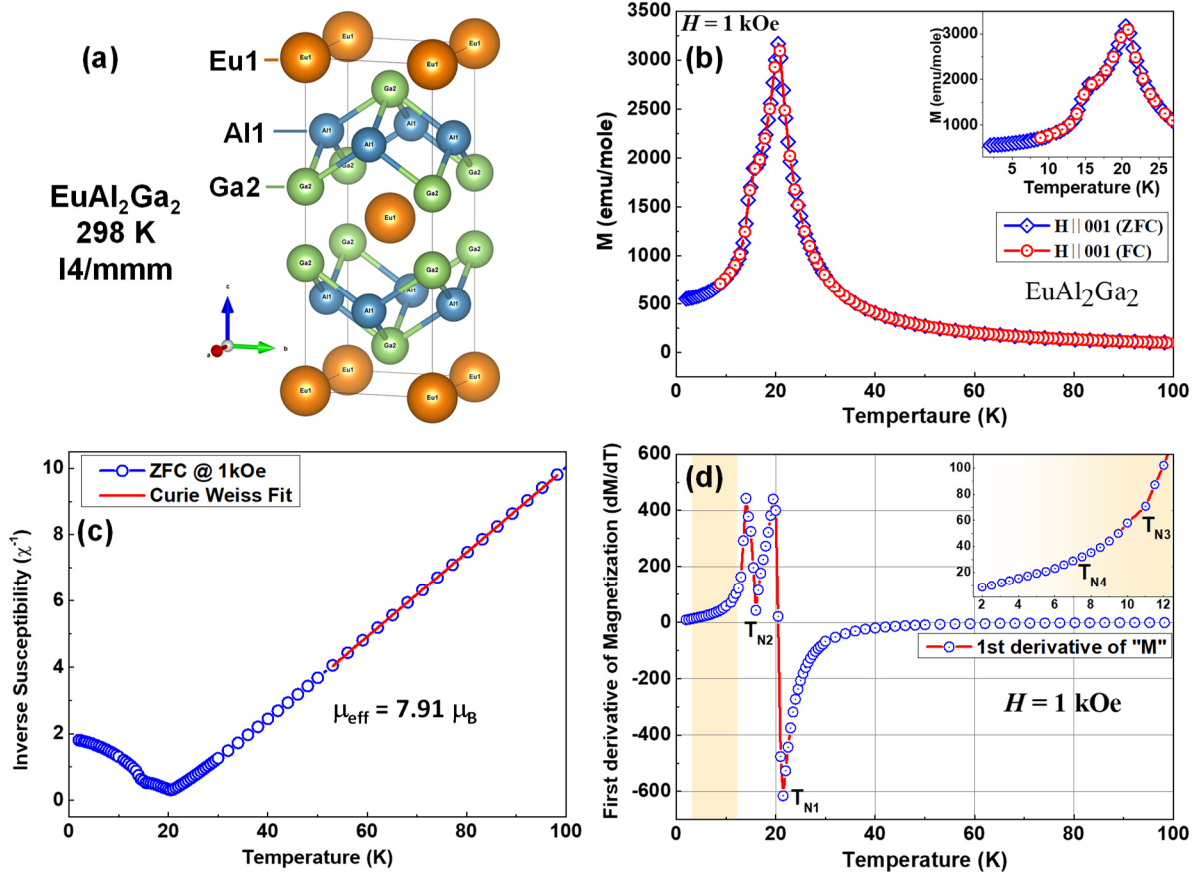


Figure 1: (a) Tetragonal structure of EuAl_2Ga_2 at 298K having the centrosymmetric $I4/mmm$ space group. (b) Temperature dependent zero field cooled, field cooled dc magnetization observed at 1k Oe in the temperature range of 2K – 100 K, showing the antiferromagnetic nature due to Eu^{2+} ion; (c) Inverse susceptibility obtained by ZFC curve; a Curie-Weiss model was fitted to the data between 55 and 100 K (red line). (d) first derivative of magnetization showing the transition temperatures of the material at $T_{N1} \approx 21.4$ K, $T_{N2} \approx 15.78$ K, $T_{N3} \approx 11.02$ K, $T_{N4} \approx 7.45$ K.

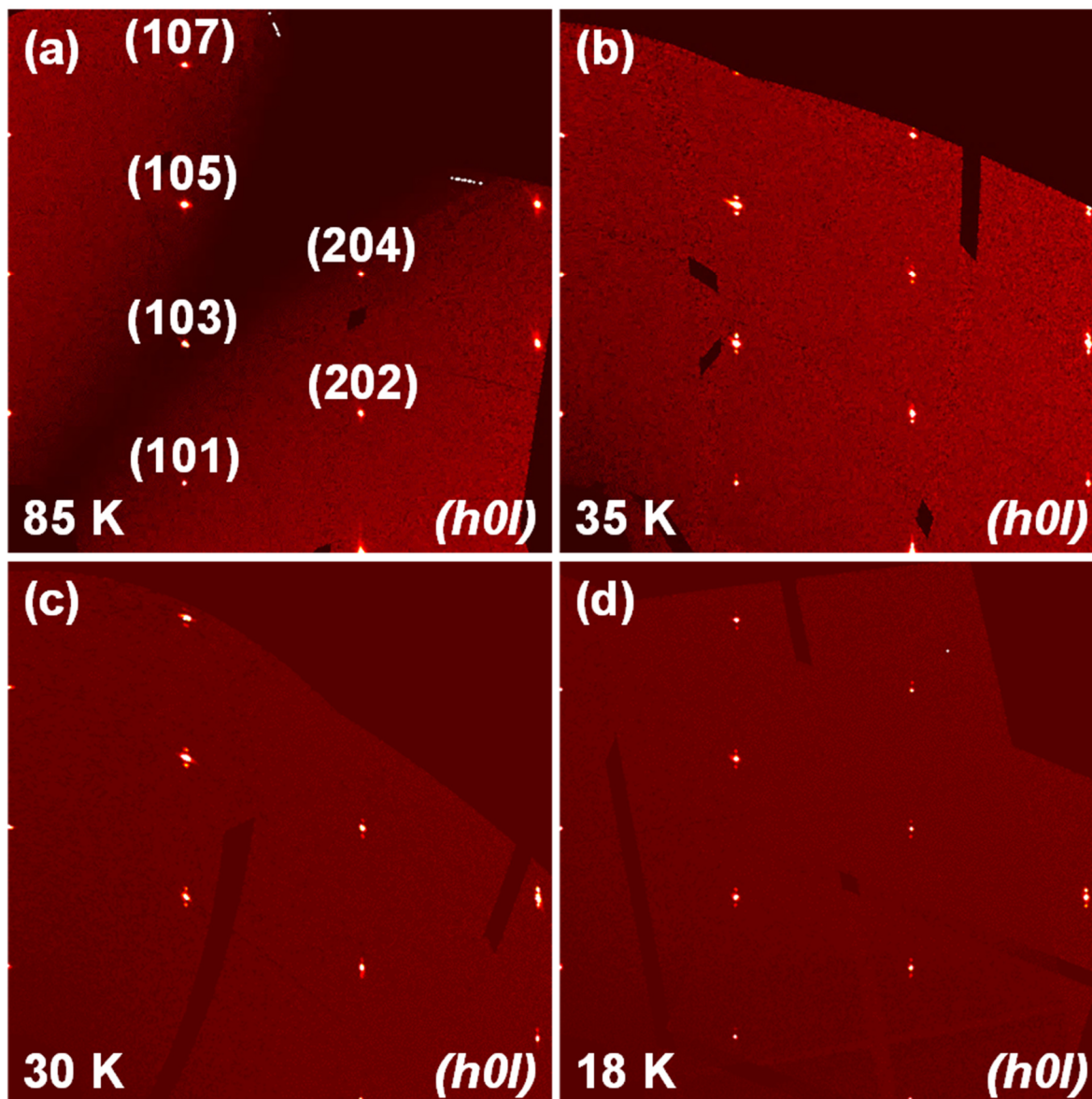


Figure 2: $(h\ 0\ l)$ Sections of reciprocal space reconstructed from SXRD data measured on EuAl_2Ga_2 at (a) $T = 85\ \text{K}$, (b) $T = 35\ \text{K}$, (c) $30\ \text{K}$, and (d) $18\ \text{K}$. Dark areas are due to insensitive parts of the detector.

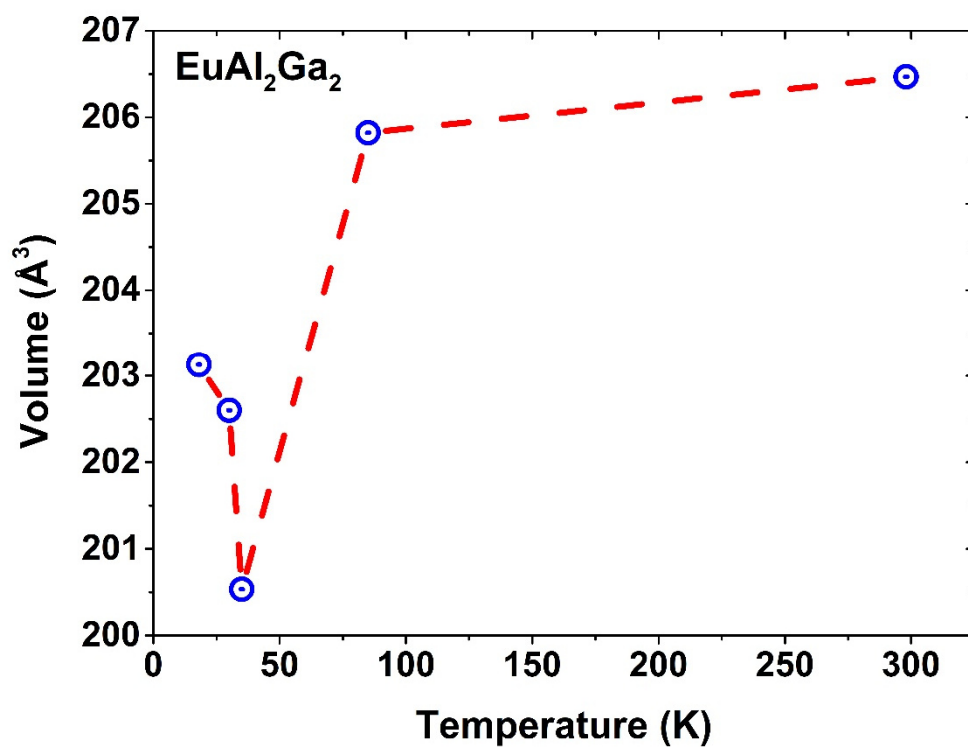


Figure 3: Temperature dependence of the volume of the unit cell.

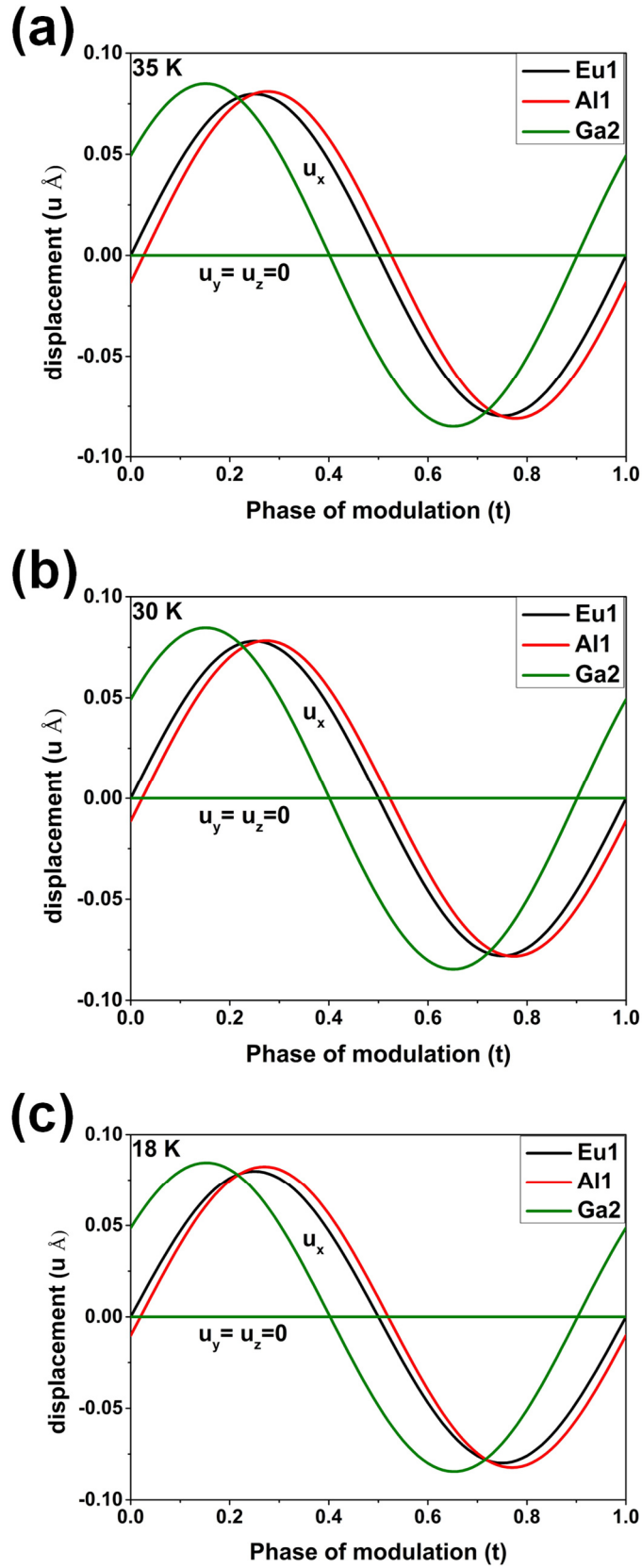


Figure 4: t-plot of the modulation functions for the displacement of atoms Eu1, Al1 and Ga2 at 35 K, 30K, 18K for superspace group $Immm(00\gamma)s00$.

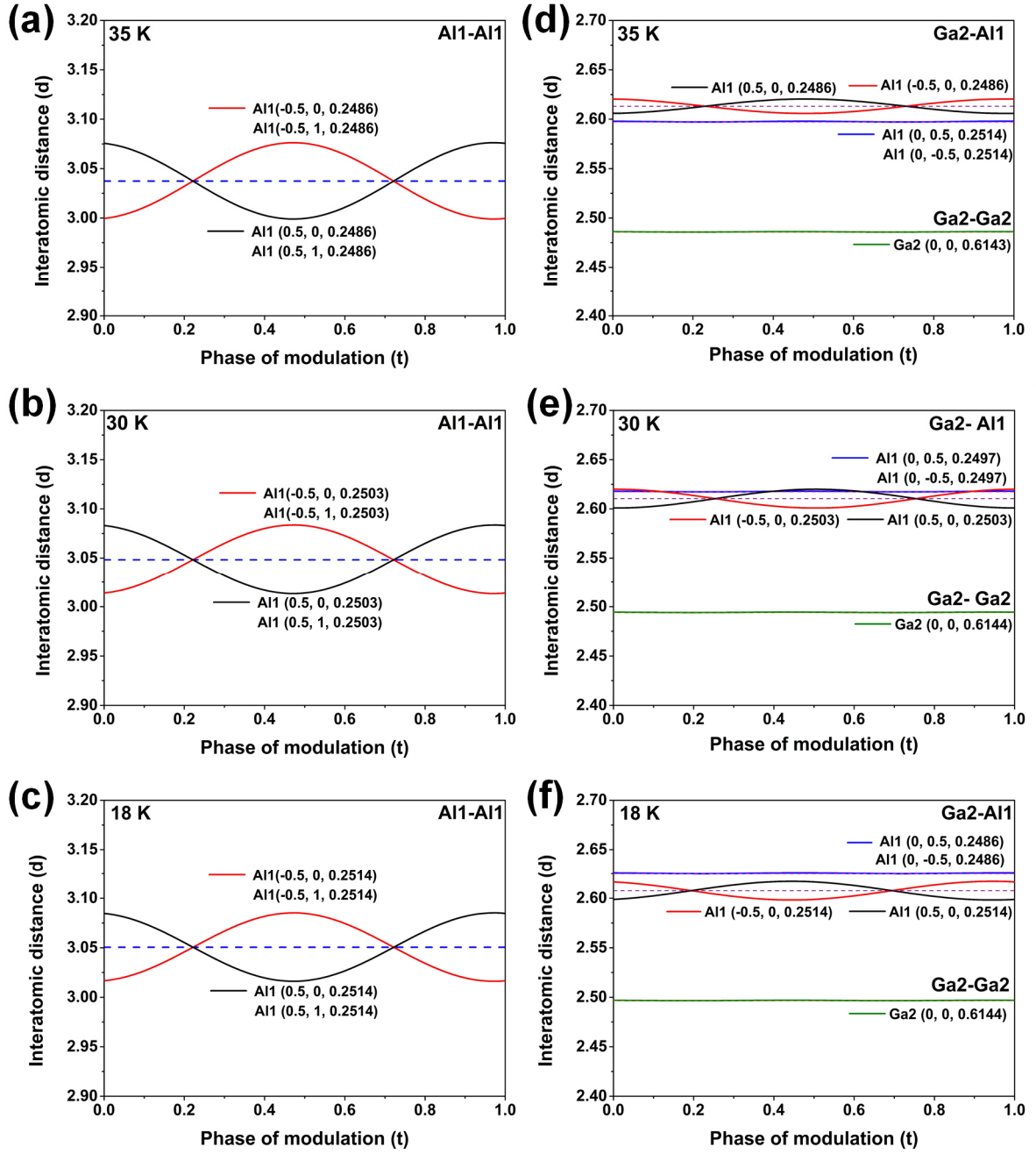


Figure 5: t-plot of interatomic distances (Å) $d[Al1-A11]$, $d[Al1-Ga2]$, $d[Al1-Ga2]$ at 35K, 30 K and 18 K for superspace group $Immm(00\gamma)s00$. Compare to Figure 6.

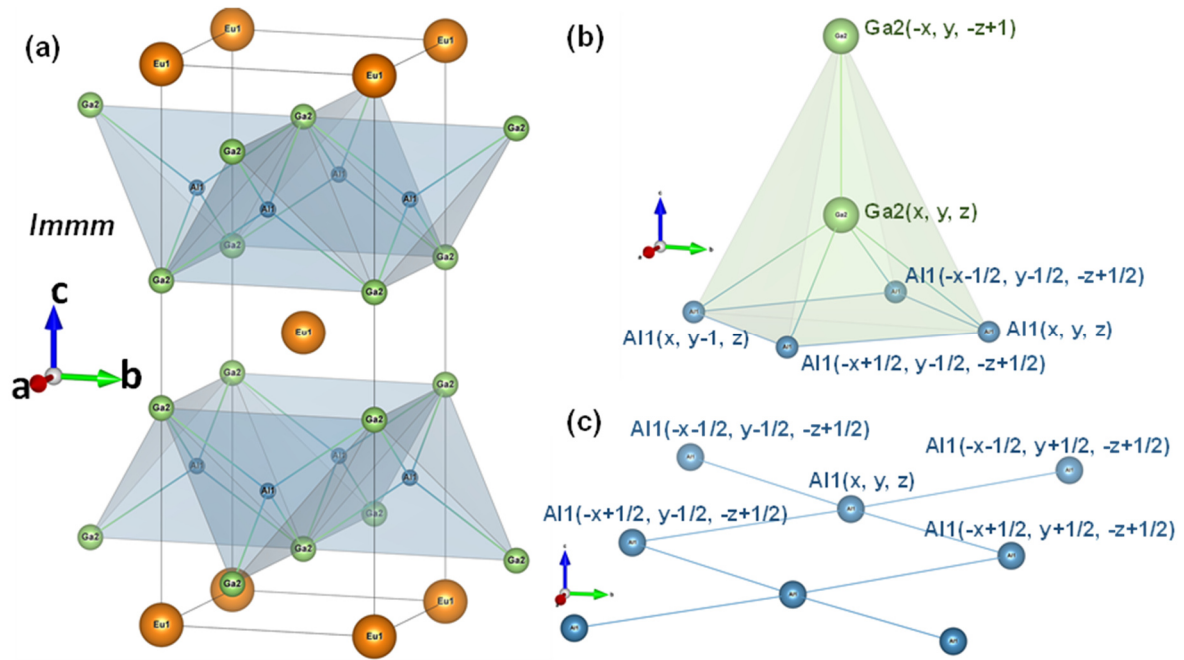


Figure 6: Crystal Structure of EuAl_2Ga_2 having orthorhombic structure with $Immm$ symmetry at 18 K (a) Polyhedral view of Al_1 - Ga_2 atoms; (b) Neighbouring atoms of Ga_2 for which the CDW modes between Ga_2 - Ga_2 and Ga_2 - Al_1 atoms are shown in figure 5; (c) neighbouring Al atoms of Al_1 for which the Al_1 - Al_1 layers shows largest modulation of interatomic distances causing CDW in the material.